

ELECTRONIC SUPPLEMENTARY INFORMATION

Thermal and chemical decomposition of di(pyrazine)silver(II) peroxydisulfate and unusual crystal structure of a Ag(I) by-product

Piotr J. Leszczyński*, Armand Budzianowski, Łukasz Dobrzycki, Michał K. Cyrański, Mariana Derzsi, and Wojciech Grochala*

Contents

S1. Reagents and synthesis.

S2. Instrumentation and experimental methodology.

S3. Structure solution and refinement.

S4. Computational methodology.

S5. Crystallographic data for monoclinic $[Ag(pyrazine)_2]S_2O_8$ (C2/c) from powder X-ray diffraction ($T=25^\circ C$) as compared to those published by Manson et al. (Ref.4).

S6. Unit cell parameters for monoclinic $[Ag(pyrazine)_2]S_2O_8$ (C2/c), $[Ag(pyrazine)_2](S_2O_8)(H_2O)$ (two C2/c polymorphs) from powder X-ray diffraction ($T=25^\circ C$) coming from evolution of the samples of $[Ag(pyrazine)_2]S_2O_8$ in time. Unit cell parameters for monoclinic $[Ag(pyrazine)_2](HSO_4)_2(H_2O)_{1/2}$ (P2₁/c) coming from pyrolysis of $[Ag(pyrazine)_2]S_2O_8$ for 24 hrs at $95^\circ C$ ($T=25^\circ C$).

S7. Crystallographic data for orthorhombic $[(Ag(I)(pyz))_5(H_2O)_2(HSO_4)_2(H(SO_4)_2)]$ from single crystal X-ray diffraction ($T=25^\circ C$) as compared to those for $[Ag(I)(pyz)]_4[Ag(II)(pyz)](H_2O)_2(HSO_4)_2(SO_4)_2$ published by Sun et al. ($T=25^\circ C$, Ref.33).

S8. Analysis of valence state of Ag in the compound claimed to be $[Ag(I)(pyz)]_4[Ag(II)(pyz)](H_2O)_2(HSO_4)_2(SO_4)_2$ published by Sun et al. ($T=25^\circ C$, Ref.33).

S9. Results of DFT calculations for $[Ag(pyrazine)_2]S_2O_8$.

S10. Results of EGA (MS 1 K/min scan & IR 3 K/min scan) for gases evolved during thermal decomposition of $[Ag(pyrazine)_2]S_2O_8$, as well as IR spectra and XRDPs for solid residues.

References.

S1. Reagents and synthesis.

Ammonium peroxydisulfate (99.9%) was obtained from Peroxid (Germany); benzene (anhydrous 98.8%); potassium peroxydisulfate (99.99%); pyrazine (99.9+%); silver acetate (99.0%); silver nitrate (ACS reagent 99.0%) silver trifluoroacetate (99.99+%) and tris(pentafluoroethyl)-amine (96%) were from Aldrich.

Typical scale: 12.5 mM of pyrazine (1.000 g), 5.6 mM of silver trifluoroacetate (1.237 g), 46 mM of ammonium peroxydisulphate (10.497 g). Pyrazine and ammonium peroxydisulphate were dissolved in 15 ml of MiliQ water ($2^\circ C$), silver trifluoroacetate was dissolved in 5 ml of MiliQ water ($2^\circ C$), solutions were mixed and brown complex started to deposit slowly. Reaction was conducted for 24 hrs at $2^\circ C$ leading to fine brown powder.

4.8 mmol of a crude product was first centrifuged for 3 min at acceleration of 3000 g and then the insoluble brown complex was shaken with cold aqueous solution of potassium peroxydisulfate and centrifuged again. The filtration procedure was repeated six times while rinsing the product with cold water (6x6 ml). Product was dried in vacuum at 0.1mm Hg for 24hrs. A typical yield after purification was only 11-15 % with respect to starting Ag(I) reagent. The purity of obtained product has been verified with powder XRD, IR/Raman spectroscopy, elemental analysis, and magnetic susceptibility measurements. Pure product is not soluble in any of ca. 20 common organic solvents tested. Product has been stored at $-35^\circ C$ in darkness to minimize decomposition.

When synthesis is conducted in the presence of large excess KNO_3 , $KClO_4$, K_2SO_4 , KF , KHF_2 , KBF_4 , or KCF_3COO , and the amount of $(NH_4)_2S_2O_8$ used is for quantitative redox reaction only (no excess), the insoluble dark-coloured derivatives of $Ag(II)(pyz)_2$ do not form. This is not due to partial decomposition of $(NH_4)_2S_2O_8$ via oxidation of ammonium cations to nitrate anions,¹ since similar fate of reaction has been observed when $K_2S_2O_8$ was used as oxidant.

WARNING! Samples of $[\text{Ag}(\text{pyrazine})_2]\text{S}_2\text{O}_8$ may vigorously decompose realising much gaseous products when at mechanical shock or during milling.

S2. Instrumentation and experimental methodology.

Elemental analysis Samples of $[\text{Ag}(\text{pyrazine})_2]\text{S}_2\text{O}_8$ complex were analyzed for C, H, N and S content with an elemental combustion (240 PERKIN ELMER) analyzer at detectability of 0.2 wt% and a typical uncertainty of 0.3 wt% for every element. The silver content in peroxydisulfate complex was determined by weight as silver chromate using an accurate method described by Pendse *et al.*² Theoretical values are: Ag 23.4; C 20.9; H 1.8; N 12.2; S 13.9. The average values of two independent experimental measurements are: Ag 23.4; C 20.4; H 1.8; N 12.2; S 13.4 (using ammonium peroxydisulfate for oxidation of Ag^+) and Ag 22.9; C 13.6; H 1.7; N 9.0; S 16.4 (using potassium peroxydisulfate).

FT-IR spectroscopy Infrared absorption spectra of 1.5 mg samples were obtained with Vertex 80 v BRUKER vacuum FT-IR spectrometer in 256 scans using AgCl windows for near- and mid-IR ($7000\text{-}500\text{ cm}^{-1}$) and Polyethylene windows for far-IR ($700\text{-}50\text{ cm}^{-1}$).

The infrared spectrum of $[\text{Ag}(\text{pyrazine})_2]\text{S}_2\text{O}_8$ complex between $1350\text{-}400\text{ cm}^{-1}$ was previously reported by Matthews *et al.*³ In this region our spectra and these reported by Manson *et al.*⁴ are very similar to those reported by Matthews *et al.*³ however our spectrum has been collected in wider range ($3800\text{-}50\text{ cm}^{-1}$) (see Fig. 1). Bands assigned to pyrazine (cm^{-1}): 3150 (m, ν C-H); 1496 (w, ν C-C); 1485 (w, ν C-C); 1474 (w, ν C-C); 1433 (m, ν C-C); 1427 (m, ν C-C); 1350 (w, δ C-H); 1221 (m, ν C-N); 1163 (m, ν C-N); 1121 (m, ν C-N); 1096 (w, ν C-N); 1079 (w, ν C-N); 1041 (s, ν C-N); 1010 (w, δ C-H); 974 (w, δ C-H); 855 (w, γ C-H); 820 (m, γ C-H); 801 (m, γ C-H); 470 (s, γ C-H); 436 (m, γ C-H); 355 (w, γ C-H). Bands assigned to peroxydisulfate ion (cm^{-1}): 1294 (s, br, ν $-\text{SO}_2-$); 1280 (sh, ν $-\text{SO}_2-$); 1235 (s, b, ν $-\text{O}-\text{SO}_2-\text{O}-$); 1052 (s, ν $\text{S}=\text{O}$); 685 (s, br, ν S-O); 673 (s, br, ν S-O); 581 (s, ν S-O); 562 (s, ν S-O); 554 (s, ν S-O). Broad band between $3500\text{-}3000\text{ cm}^{-1}$ indicates a presence of occluded moisture.

Raman spectroscopy Raman scattering spectra were measured with dispersive T 64000 Raman spectrometer (JOBIN YVONNE-SPEX) equipped with 50 mm optical lens microscope BX40 (OLYMPUS) at a backscattering geometry. The 647.09 nm (red) excitation line of the Ar/Kr laser was used. All samples were sealed inside 1 mm quartz capillary. The Raman spectrum in the ($2600\text{-}300\text{ cm}^{-1}$) region contained modes assigned to pyrazine and a peroxydisulfate ion as ligands in the coordination sphere of $[\text{Ag}(\text{pyrazine})_2]\text{S}_2\text{O}_8$ complex. Modes assigned to pyrazine (cm^{-1}) are: 1592 (m, ν , A_g mode); 1037 (w, ν , A_g mode); 965 (w, ν , B_{1g} mode), whereas modes assigned to peroxydisulfate ion (cm^{-1}) are: 1592 (m); 1079 (w, ν_s S-O mode); 660 (w); 644 (w); 594 (w, δ SO_3^- mode); 457 (w); 433 (w).

Magnetic susceptibility measurements The magnetization measurements were performed using a commercial “Quantum Design”-made SQUID magnetometer in 4.5-300 K range. In the Zero Field Cooling (ZFC) regime samples were cooled down to 4.5 K without magnetic field before starting measurement and in the Field Cooling (FC) regime magnetic field of 1 kOe was applied. The back-ground subtraction procedure was done for each experimental points, subtracting separately measured empty Teflon[®] capsule.

The almost single-phase, polycrystalline samples of $[\text{Ag}(\text{pyrazine})_2]\text{S}_2\text{O}_8$ complex were characterized by measuring thermal variation of magnetic susceptibility (χ_m vs. T). χ_m gradually increases as the temperature is lowered, reaching a broad maximum at $T_{\text{Néel}} = 49\text{ K}$. The relatively high value of $T_{\text{Néel}}$ suggests strong AFM interactions in each 2D square lattice of Ag^{2+} ions in the intrinsic structure of $[\text{Ag}(\text{pyrazine})_2]\text{S}_2\text{O}_8$ complex. Our results thus agree well with those reported by Manson *et al.*³

TGA/DSC/Q-MS/FT-IR The thermal decomposition of the $[\text{Ag}(\text{pyrazine})_2]\text{S}_2\text{O}_8$ complex samples (mass loss, heat flow) was monitored in the temperature range of $30\text{-}400^\circ\text{C}$ at heating rate of $10^\circ\text{C}/\text{min}$ in the ultra pure argon (6.6N) stream using STA (simultaneous thermal analyzer) 409 from NETZSCH. Alumina (Al_2O_3) crucibles were used. The evolved gases were analyzed with a Q-MS 403C Aëolos PFEIFFER-VACUUM mass spectrometer (connected to STA via a quartz capillary). The transfer line connecting the thermal analyzer and Q-MS was preheated up to 200°C to avoid condensation of low-boiling residues. The process of thermal decomposition was conducted on a Teflon[®] plate and documented using a CANON EOS 30D digital camera. Temperature of the heated sample was measured using an infrared thermometer (pyrometer).

Single crystal XRD were measured at 100 K on a KM4CCD κ -axis diffractometer with graphite-monochromated MoK_α radiation. The crystal was positioned at 62 mm from the CCD camera. 649 frames were measured at 0.52° intervals with a counting time of 30 sec. The data were corrected for Lorentz and polarization effects. Empirical correction for absorption was applied.⁵ Data reduction and analysis were carried out with the Oxford Diffraction programs.⁶ The structure was solved by direct methods.⁷ The refinement using WinGX⁸ and SHELXL⁹ was based on F^2 for all reflections except those with very negative F^2 . Weighted R factors wR and all goodness-of-fit S values are

based on F^2 . The $F_o^2 > 2\sigma(F_o^2)$ criterion was used only for calculating R factors. Scattering factors were taken from Tables 6.1.1.4 and 4.2.4.2 in Ref.10.

Powder XRD measurements The BRUKER D8 Discover diffractometer with the parallel beam of 18 mm length from CuK_α X-ray tube ($\lambda=1.5406 \text{ \AA}$) and the Vantec detector have been used to record most of the diffraction patterns from the samples with the step size lower than 0.02 deg and diffraction range wider than 10-90 deg (and measuring time of 12 sec per point). Only selected samples were measured using PANalytical Diffractometer X'Pert PRO with the radius set to 240 mm. The parallel beam of 27 mm length has been obtained using the W/Si parabolic mirror. The CoK_α X-ray tube ($\lambda \text{ K}_{\alpha 1}= 1.78901 \text{ \AA}$, $\lambda \text{ K}_{\alpha 2}=1.79290 \text{ \AA}$, ratio 0.5) powered by 40kV and 40 mA. Continuous 2theta scan with rotated capillary (DSH method) using the the PIXcel detector have been used to record the diffraction from the samples. All powder XRD measurements were carried out at room temperature.

S3. Structure solution and refinement.

Crystal twinning and single crystal structure refinement of $[(\text{Ag}(\text{I}(\text{pyz}))_5(\text{H}_2\text{O})_2(\text{HSO}_4)_2(\text{H}(\text{SO}_4)_2)]$. The measured crystal contained two differently oriented domains. The orientation of both components suggests twinning but also the accidental association of two single crystals could be considered. The twinning could occur due to the specialized metric of the crystal lattice. The lattice symmetry of the crystal is orthorhombic but if a is doubled the lattice becomes pseudo-tetragonal with the twin obliquity equal to $0.14(1)^\circ$ whereas the 0° obliquity stands for the exact tetragonal symmetry of the lattice. So, the twinning occurs as a rotation along [001] axis, for example, causing almost ideal overlap of every second reflection from two domains and leaving the rest reflections separated. However the non-zero obliquity and the low-quality of the crystal caused non-exact overlapped of equivalent reflections. Nevertheless the applying of the twin matrix during the structure refinement lowered the final discrepancy factors and values of residual electron density to the reasonable levels.

During the structure refinement the "HKL F 5" option was used. The ratio of both components was refined and yielded 0.184(1):0.816(1). After the refinement converged the data were merged using WinGX.⁸ Because of the twinning and high absorption of the crystal some constraints and restraints were used during the structure refinement. All hydrogen atoms were located geometrically and their position and temperature factors were not refined. The hydrogen H21 atom of the hydrogen bis-sulfate group was positioned exactly between O21 and O21 atoms related by $(x, y, 3/2-z)$ reflection. The water molecule was refined as a rigid body with fixed geometry. Only the rotation was free to refine leading to the reasonable hydrogen bond network formation. All non-hydrogen atoms were refined with anisotropic thermal parameter, however oxygen O24 and some nitrogen - N11, N14, N34 and carbon - C12, C15, C16, C25, C26, C32, C33, C35, C36 atoms were refined to approximate isotropic behaviour with the "ISOR 0.004" instruction.

The refined structure is in fact the superstructure. In the crystal lattice the pseudo translation symmetry along (010) could be found. Applying of such a symmetry would cause halving of the b unit cell parameter. Such an approach would lead to the averaged structure with some Ag-pyrazine ribbons statically disordered. However due to heavy Ag moiety presence the reflections are strong enough to find the proper unit cell parameters leading to the superstructure.

Powder XRD analysis The phase quality analyses were made with EVA.¹¹ The background from each diffractogram has been subtracted and intensity normalization was been applied allowing for separation of reflexes from the main product and impurities. Each pattern has been compared with PDF patterns from the ICDD data base.¹² Pyrazine (in any of its two known polymorphic structures^{13,14}), AgO (in two structure types)¹⁵, and metallic silver^{16,17}, were absent.

The structure refinement of $[\text{Ag}(\text{pyrazine})_2]\text{S}_2\text{O}_8$ was made in JANA¹⁸ using the Pseudo-Voigt profiles and Berar-Baldinozzi asymmetry. The crystal structure previously obtained from a synchrotron powder diffraction,⁴ has been used as a starting model. Restraints for distances, angles and torsion angles have been applied for two pyrazinium molecules, one SO_4 moiety and the O-O bond. The values for restraints has been taken from the starting model⁴ with a tolerance for the length of 0.001 \AA and of 0.01° for angles and torsion angles. The equivalent isotropic temperature factors were averaged for all C & N atoms. The isotropic temperature factors for hydrogen were calculated as 120% of isotropic temperature factors of carbon atoms.

As the X-ray diffraction pattern (XRDP) of our samples was changing in time, two new sets of reflexes were found with their intensities correlated within each set. Selected reflexes were used for indexing and space group determination using TREOR90, DICVOL91, ITO15, X-Cell, and TOPAS.^{18,23,24,25,26} The property of indexation has been checked by whole powder pattern decomposition including both the Pawley and the Le Bail methods^{27,28} using TOPAS and Material Studio software.^{29,30} Four approaches using combination of Le Bail and Pawley method with two functions of profile shape (Fundamental Parameters^{19,20,21,22} and the modified Thompson-Cox-Hastings pseudo-Voigt "TCHZ") have been applied to confirm consistence of the indexing model with the experimental data. Eventually, two monoclinic cells with extinction condition C2/c were chosen as correct solutions. These two unit cells as well as that of of $[\text{Ag}(\text{pyrazine})_2]\text{S}_2\text{O}_8$, suffice to describe evolution in time of the XRDP of our samples. The

Lorentzian crystal size was calculated for all phases. The unit cell refinement has been performed in TOPAS using two diffractograms at a time: one 129 days, and another 305 days from synthesis. For this multiphase and multidiffractogram refinement we used the Pawley method with the TCHZ profile shape.

S4. Computational methodology.

Solid-state Density Functional Theory (DFT) calculations were performed using the VASP code³¹ with the projector-augmented wave method (PAW)³². For the exchange-correlation part of the Hamiltonian, the generalized gradient approximation (GGA) in its spin density approximation variant was applied. The electronic iterations convergence was set to 10^{-7} eV by using the standard blocked Davidson algorithm and reciprocal space projection operators. The spacing between the k-points for the k-points mesh generation was *ca.* 0.2 \AA^{-1} (Monhorst pack of $2 \times 2 \times 2$). The valence electrons were described by plane waves with the kinetic energy cutoff of 600 eV, yielding satisfactory convergence of total energy. Only one scheme of magnetic ordering was analyzed in detail (AFM within sheets), as suggested from experiment.⁴

The spin-polarized GGA+U single-point calculations were performed in order to derive the electronic and magnetic structure of $[\text{Ag}(\text{pyrazine})_2]\text{S}_2\text{O}_8$ as well as the intra-sheet magnetic superexchange constant, *J*. To mimic the strongly correlated nature of the 4d electrons of Ag the value of the Coulomb integral *U* was set to 4 eV and Hund's exchange *J* to 1 eV for Ag; we have noticed that introducing *U* for the p electrons of the bridging pyrazine ligands (within the superexchange Ag–NC₄N–Ag path) has minor effect on the outcome of the calculations. The value of *J* was approximated by the difference of energy of AFM and FM configurations (which differ in the spin flip within the sheets) as customary for 2D systems (this value was divided by the number of Ag(II) cations per magnetic unit cell, *Z*=8). All calculations were done using the previously published structure of $[\text{Ag}(\text{pyrazine})_2]\text{S}_2\text{O}_8$ ⁴ without further optimizations. The $1 \times 2 \times 1$ supercell (*Z*=8) with 248 atoms was taken for calculations.

Calculations were performed on ICM supercomputers (KDM grant G34-10).

S5. Crystallographic data for monoclinic $[\text{Ag}(\text{pyrazine})_2]\text{S}_2\text{O}_8$ (C2/c) from powder X-ray diffraction (*T*=25 °C) as compared to those published by Manson *et al.* (Ref.4, supposedly room temperature).*

Chemical formula	$[\text{Ag}(\text{pyrazine})_2]\text{S}_2\text{O}_8$	
Radiation	Co, X-ray radiation, 1.79021 Å	synchrotron X-ray radiation, 0.69840 Å
2θ range & step (°)	5.01–133.97, step 0.03	2–35, step 0.005
Lattice parameters	This work	Ref.4
a (Å)	15.9964(8)	15.99695(15)
b (Å)	7.1448(2)	7.150080(64)
c (Å)	14.6110(6)	14.61384(13)
β (°)	124.9768(18)	124.95713(46)
Cell Volume (Å³)	1368.30(10)	1369.948(23)
Z	4	4
Crystal Density (g/cm³)	2.233	2.230
LP Factor	90 (not polarized)	?
Crystal Linear Absorption Coeff. (1/cm)	23.1	?
	R-Values	
R_{exp} :	0.0091	0.02729
R_{wp} :	0.0218	0.06659
R_p :	0.0143	?
GOF :	2.39	2.440
R-Bragg :	0.1433	?
Zero error :	0.02600851	?

*) Monoclinic unit cell of $[\text{Ag}(\text{pyrazine})_2]\text{S}_2\text{O}_8$ may be transformed to a quasi-tetragonal cell (*a*=14.198 Å, *b*= 14.300 Å, *c*= 27.154 Å, β = 96.305°, *V*=5479.792 Å³, *Z*=16), via a transformation using matrix (101, 020, -101). The value of *c* here reflects the separation between the $[\text{Ag}(\text{pyz})_2]$ sheets. See also Table S6.

S6. Unit cell parameters for monoclinic $[Ag(pyrazine)_2]S_2O_8$ (C2/c), $[Ag(pyrazine)_2](S_2O_8)(H_2O)$ (two C2/c polymorphs) from powder X-ray diffraction ($T=25^\circ C$) coming from evolution of the samples of $[Ag(pyrazine)_2]S_2O_8$ in time. Unit cell parameters for monoclinic $[Ag(pyrazine)_2](HSO_4)_2(H_2O)_{1/2}$ (P2₁/c) coming from pyrolysis of $[Ag(pyrazine)_2]S_2O_8$ at $95^\circ C$ for 24 hrs ($T=25^\circ C$). Cells transformed using matrix (101, 020, -101) have unit cell vectors marked with a star. (Cu radiation)

Chemical formula	$[Ag(pyrazine)_2](S_2O_8)$	$[Ag(pyrazine)_2](S_2O_8)(H_2O)$ Phase I	$[Ag(pyrazine)_2](S_2O_8)(H_2O)$ Another polymorph, II	$[Ag(pyrazine)_2](HSO_4)_2(H_2O)_{1/2}$ Phase V
Lattice parameters	This work	This work	This work	This work
a (Å)	15.99167(40)	17.4120(10)	17.98718(45)	18.4921(39)
b (Å)	7.14394(15)	7.19311(52)	7.19551(22)	7.3095(12)
c (Å)	14.60576(30)	14.76496(90)	14.84810(34)	15.2554(31)
β (°)	124.9678(12)	127.3888(55)	129.1977(12)	131.421(13)
Cell Volume (Å ³)	1367.387(57)	1469.30(20)	1489.294(73)	1546.26(20)
Z	4	4	4	4
Crystal Linear Absorption Coeff. (1/cm)	302.6(16)	302.6(16)	302.6(16)	255(18)
a* (Å)	14.149	14.456	14.367	14.190
b* (Å)	14.288	14.386	14.291	14.619
c* (Å)	27.144	28.869	29.692	30.790
β* (°)	96.32	101.78	103.98	104.478
		R-Values		
R _{exp} :		0.0113		0.0191
R _{exp} ' :		0.0313		0.0667
R _{wp} :		0.0383		0.0304
R _{wp} ' :		0.1058		0.1061
R _p :		0.0251		0.0230
R _p ' :		0.0847		0.0989
GOF :		3.38		1.59
DW :		0.46		1.32
Zero error :		-0.04140(39)		+0.0644(35)

*) For the cell obtained via a transformation matrix (101, 020, -101).

S7. Crystallographic data for orthorhombic $[Ag(I)(pyz)]_5(H_2O)_2(HSO_4)_2(H(SO_4)_2)]$ from single crystal X-ray diffraction ($T=100 K$) as compared to those for $[Ag(I)(pyz)]_4[Ag(II)(pyz)](H_2O)_2(HSO_4)_2(SO_4)_2$ published by Sun et al. ($T=25(2)^\circ C$, Ref.33).

Chemical formula	[(Ag(I)(pyz)) ₅ (H ₂ O) ₂ (HSO ₄) ₂ (H(SO ₄) ₂) ₄ [Ag(I)(pyz)] ₄ [Ag(II)(pyz)](H ₂ O) ₂ (HSO ₄) ₂ (SO ₄) ₂]	
Lattice parameters	This work	Ref.32
a (Å)	7.1273(7)	7.1428(19)
b (Å)	14.2131 (9)	14.203(4)
c (Å)	34.705 (2)	35.245(10)
Cell Volume (Å ³)	3515.6 (5)	3575.6(17)
Crystal Density (g/cm ³)	2.575	2.527
Z	4	4
Abs. coefficient (mm ⁻¹)	3.07	3.02
Crystal dimensions (mm)	0.30 × 0.25 × 0.15	0.12 × 0.10 × 0.08
Ranges hkl	h = -8→8 k = -16→16 l = -25→41	h = -8→8 k = -16→15 l = -28→41
θ _{max} / θ _{min} (deg)	25.1 / 2.9	25.0 / 1.2
Reflections/ I > 2σ(I)	3166 / 2314	3179/2897
Reflections/ param.	3166 / 78 / 271	3179 / 272 / 0
Restr		
R[F ² > 2σ(F ²)]	0.0561	0.049
wR(F ²)	0.1732	0.112
Δ _{max} / Δ _{min} (e Å ⁻³)	1.99 / -1.40	1.30 / -0.68
GOF :	1.13	1.07

S8. Analysis of valence state of Ag in the compound claimed to be [Ag(I)(pyz)]₄[Ag(II)(pyz)](H₂O)₂(HSO₄)₂(SO₄)₂] published by Sun et al. (T=25 °C, Ref.33).

According to Ref.33, one out of five Ag cations present in this complex is divalent silver, while the remaining four are monovalent. This might be possible in two cases only:

A) if Ag(II) is equivalent to Ag₃ in a genuine mixed-valence compound (note, there are TWO Ag₁ and TWO Ag₂ cations in the structure and ONE Ag₃ cation)

B) or if d hole of Ag(II) is spread over all five Ag cations, rendering this complex an intermediate-valence one.

Case A) seems impossible because the coordination sphere of Ag₃ is very similar to those of Ag₁ and Ag₂ (see Table below) with the average Ag-N distances taking very similar values for all three types of Ag atoms (2.175 Å for Ag₁, 2.180 Å for Ag₂, 2.181 Å for Ag₃). The same is true for the Ag-O distances (2.594 Å for Ag₁, 2.709 Å for Ag₂, 2.625 Å for Ag₃), while Ag-ligand distances shorter by at least 0.2 Å are expected for Ag(II) as compared to Ag(I).

Ag1—N14 ⁱ	2.174 (6)
Ag1—N11	2.176 (6)
Ag1—O12	2.594 (5)
Ag2—N24i	2.168 (7)
Ag2—N21	2.193 (7)
Ag2—O22	2.709 (6)
Ag3—N34i	2.176 (9)
Ag3—N31	2.187 (8)
Ag3—O22	2.625(5)
Ag2—Ag3	3.3352 (6)

Symmetry codes: (i) x+1, y, z.

The hypothesis on a purely Ag(I)-character of the complex is corroborated by analysis of hydrogen bonding (see Table below) which points to the presence of H21 proton engaged in a short (2.427 Å) symmetric hydrogen bonding between two hydrogensulfate anions.

D—H...A	D—H	H...A	D...A	D—H...A	Comment on D and A
O1—H1B...O13	1.00	1.82	2.801 (7)	166.1	water – HSO ₄ ⁻ ion
O1—H1A...O24	1.00	1.77	2.755 (7)	171.2	water – [H(SO ₄) ₂] ²⁺ ion
O11—H11...O1 ⁱ	0.84	1.82	2.647 (7)	165.7	HSO ₄ ⁻ ion – water

Although the only three known mixed-valence Ag(I)/Ag(II) systems (fluorosulfate,³⁴ hexafluoroantimonate,³⁵ and a more complex system involving organic ligand³⁶) are of mixed- and not intermediate-valence character, yet option B) (intermediate valence) should also be taken into account. However, B) seems out of question since an intermediate valence system would be metallic in nature, with all associated optical properties such as metallic luster etc. This is not observed experimentally. In addition, the published luminescence spectrum of the claimed mixed-valence complex³² is very similar to the spectra of pyrazine-Ag(I) compounds.³⁷

O21—H21...O21 ⁱⁱ	1.21	1.21	2.427	180.0	[H(SO ₄) ₂] ³⁻ ion, intermolecular symmetric H bond
-----------------------------	------	------	-------	-------	--

Symmetry codes: (i) x+1, y, z; (ii) x, y, -z+3/2. Note, positions of H are subject to large error.

S9. Results of DFT calculations for [Ag(pyrazine)₂]S₂O₈.

Absolute values of spin on all atoms point to large share of unpaired electron density on two pyrazine ligands (49.4 %), comparable to the one on Ag(II) cation (49.0 %); negligible contribution is found from peroxodisulfate anion (1.7 %).

The calculated value of J is -29.6 meV per FU and this it reproduces very well the sign of superexchange coupling constant (*i.e.* the observed antiferromagnetism) but it is 6 times larger from the experimental value of -4.6 meV.⁴ The overestimation of J by up to one order of magnitude is a typical shortcoming of DFT methods.³⁸

Atom	Magnetization (e)	Moiety	Absolute spin (e)	Spin share (%)
Ag	±0.355	Ag	0.355	49.0
N	±0.076 to ±0.080	2 N ₂ C ₄ H ₄	2 x 0.179	49.4
C	±0.005 to ±0.006	S ₂ O ₈ ²⁻	0.012	1.7
H	0.000 to ±0.001	Total	0.724	100.0
S	±0.001			
O(terminal)	±0.003 to ±0.004			
O(peroxo bridge)	0.000			

Rounding error 0.1 %

S10. Results of EGA (MS 1 K/min scan & IR 3 K/min scan) for gases evolved during thermal decomposition of [Ag(pyrazine)₂]S₂O₈, as well as IR spectra and XRDPs for solid residues.

63 min 93 deg C

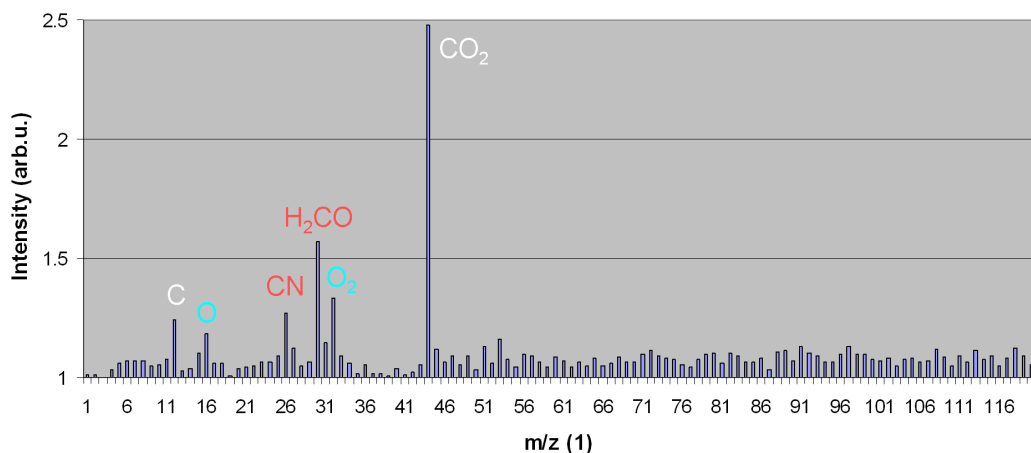


Fig.S1 Quadrupole mass spectrum of gases evolved during thermal decomposition of [Ag(pyrazine)₂]S₂O₈ complex (taken at 93 °C, I dec. step).

197 min 228 deg C

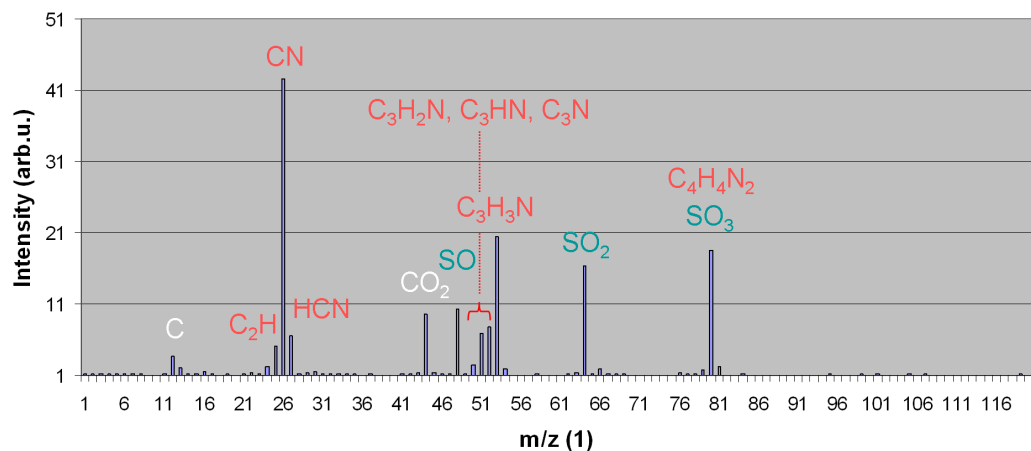


Fig.S2 Quadrupole mass spectrum of gases evolved during thermal decomposition of $[\text{Ag}(\text{pyrazine})_2]\text{S}_2\text{O}_8$ complex (taken at 228 °C, II dec. step).

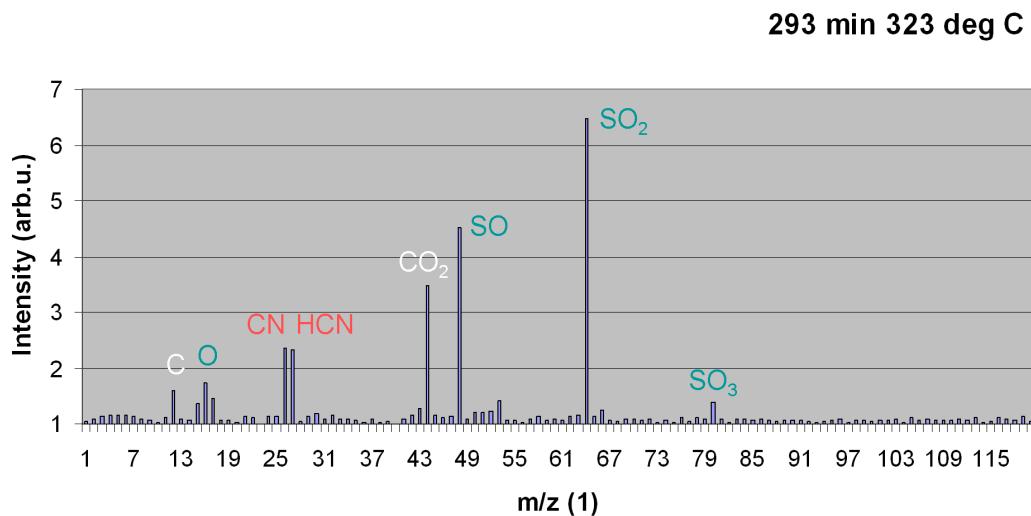


Fig.S3 Quadrupole mass spectrum of gases evolved during thermal decomposition of $[\text{Ag}(\text{pyrazine})_2]\text{S}_2\text{O}_8$ complex (taken at 323 °C, III dec. step).

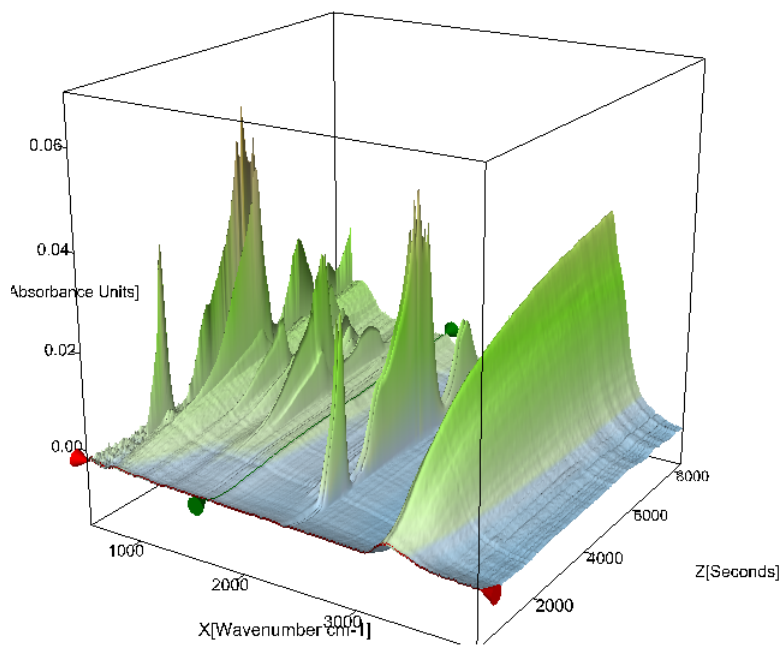


Fig.S4 3D FTIR spectrum of gases evolved during thermal decomposition of $[\text{Ag}(\text{pyrazine})_2]\text{S}_2\text{O}_8$ complex. The growing OH stretching band comes mostly from ice forming on the LN₂-cooled detector.

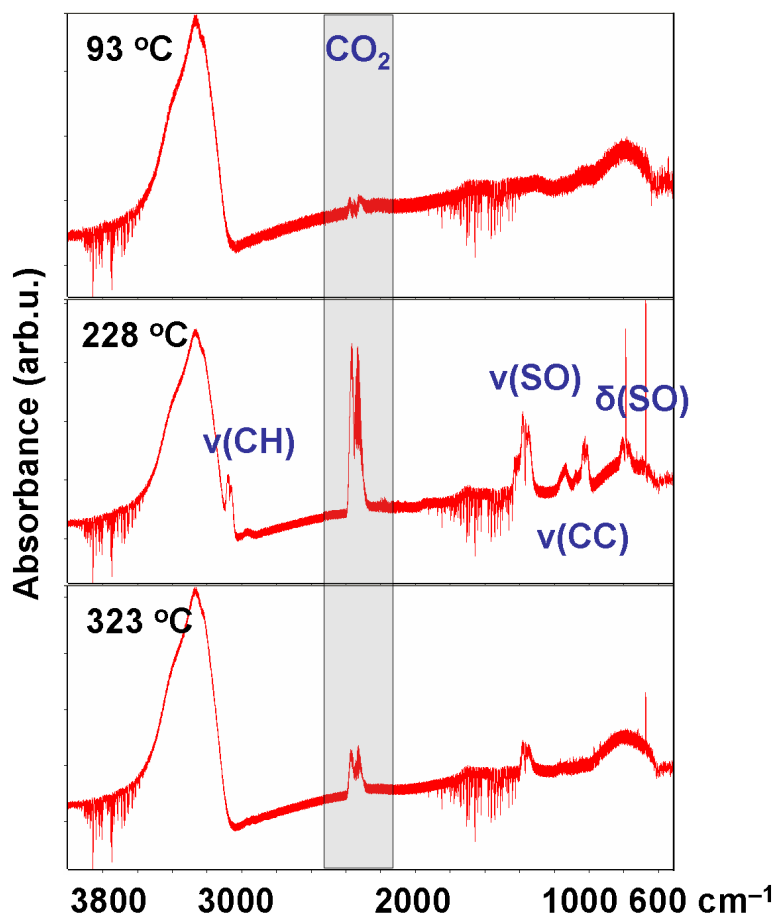


Fig.S5 FTIR spectrum of gases evolved during thermal decomposition of [Ag(pyrazine)₂]S₂O₈ complex (taken at 93 °C, I dec. step, 228 °C, II dec. step and 323 °C, III dec. step).

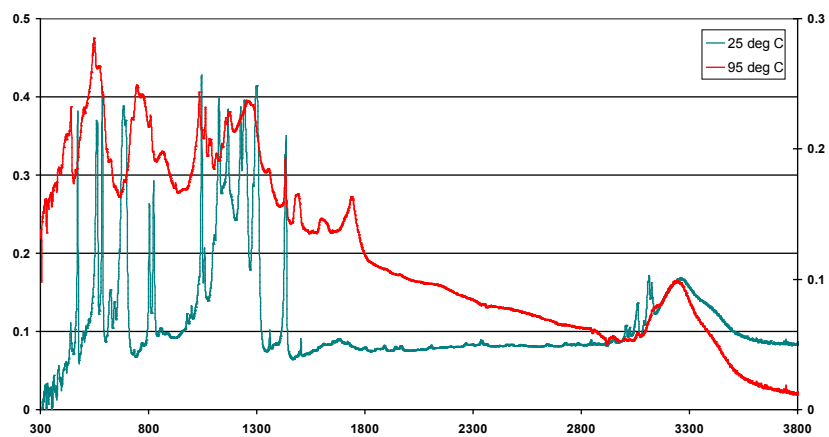


Fig.S6 FTIR spectrum of solid residue obtained during thermal decomposition of [Ag(pyrazine)₂]S₂O₈ complex at 95 °C for 24 hrs and cooled to RT, as compared to the one measured for [Ag(pyrazine)₂]S₂O₈ at RT.

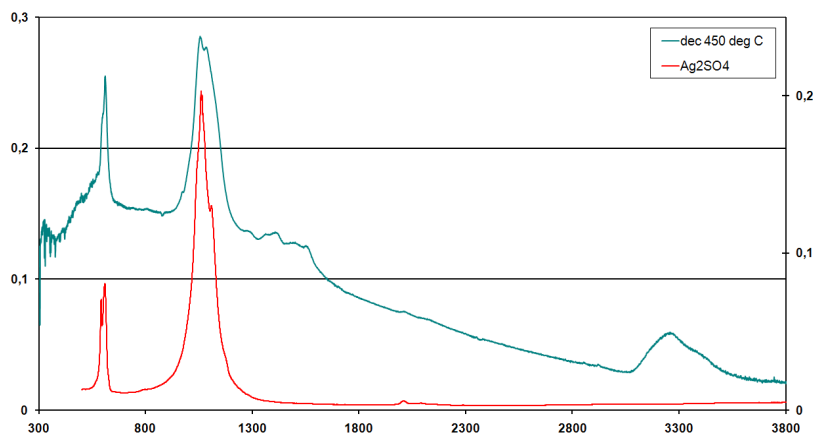


Fig.S7 FTIR spectrum of solid residue obtained during thermal decomposition of $[\text{Ag}(\text{pyrazine})_2]\text{S}_2\text{O}_8$ complex at 450 °C for 24 hrs and cooled to RT, as compared to the FTIR spectrum of Ag_2SO_4 .

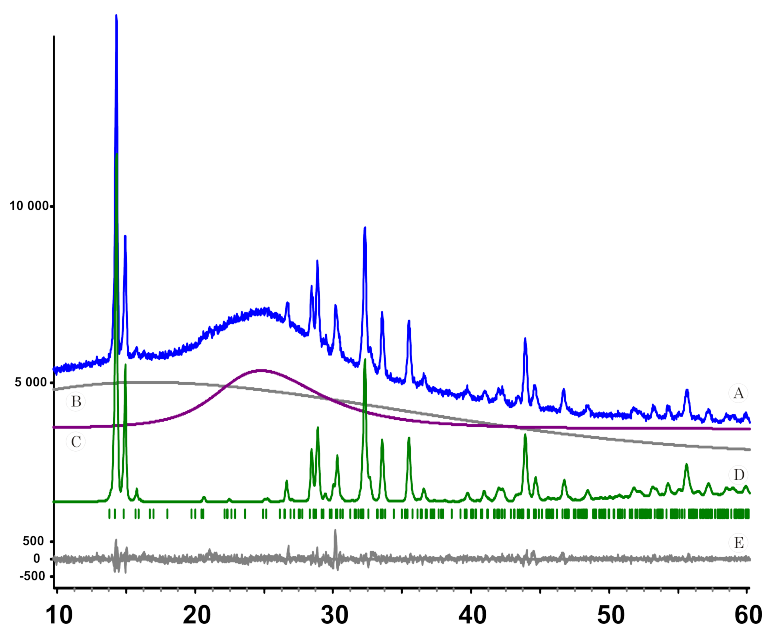


Fig.S8 XRD of solid residue obtained during thermal decomposition of $[\text{Ag}(\text{pyrazine})_2]\text{S}_2\text{O}_8$ complex at 95 °C for 24 hrs and cooled to RT. A) experimental XRDP, B) background, C) amorphous hump, D) contribution from phase V and set of respective hkl positions, E) differential pattern.

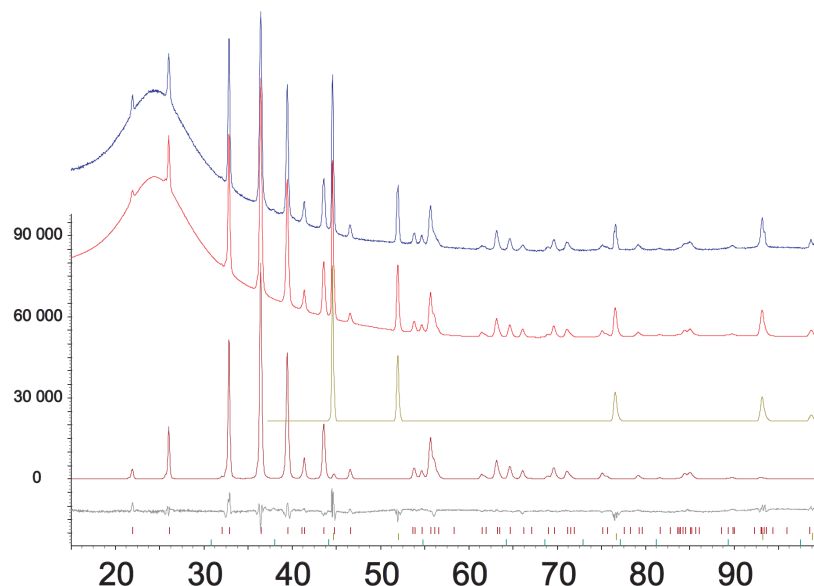


Fig.S9 XRD of solid residue obtained during thermal decomposition of $[\text{Ag}(\text{pyrazine})_2]\text{S}_2\text{O}_8$ complex at 450 °C for 24 hrs and cooled to RT. From top to bottom: experimental XRDP, fitted XRDP, contribution from Ag, contribution from Ag_2SO_4 , differential pattern, two sets of respective hkl positions.

References.

1. C. V. King, *J. Am. Chem. Soc.* **1928**, 50, 2080.
2. G. H. Pendse, H. D. Bhargava, and B. R. Sant, *J. Anal. Chem., Fresenius*, **1958**, 160, 188.
3. R. W. Matthews, R. A. Walton, *Inorg. Chem.*, **1971**, 10, 1433.
4. J. L. Manson, K. H. Stone, H. I. Southerland, T. Lancaster, A. J. Steele, S. J. Blundell, F. L. Pratt, P. J. Baker, R. D. McDonald, P. Sengupta, J. Singleton, P. A. Goddard, Ch. Lee, M. -H. Whangbo, M. M. Warter, Ch. H. Mielke, and P. W. Stephens, *J. Am. Chem. Soc.*, **2009**, 131, 4590.
5. CrysAlis RED, Oxford Diffraction Ltd., Version 1.171.33. **2010**. Empirical absorption correction using spherical harmonics, implemented in SCALE3 ABSPACK scaling algorithm.
6. CrysAlis CCD, Oxford Diffraction Ltd., Version 1.171.33, **2010**.
7. G. M. Sheldrick, *Acta Crystallogr.* **1990**, A46, 467.
8. L. J. Farrugia, *J. Appl. Cryst.*, **1999**, 32, 837.
9. G. M. Sheldrick, *SHELXL93. Program for the Refinement of Crystal Structures.*, Univ. of Göttingen, Germany **1993**.
10. *International Tables for Crystallography*, Ed. A. J. C. Wilson, Kluwer, Dordrecht, **1992**, Vol.C.
11. Diffrac+, Eva (**2002**): EVA - User's Manual, Bruker AXS, Karlsruhe, Germany.
12. J. Faber and T. Fawcett, *Acta Cryst.*, **2002**, B58, 325, and The International Centre for Diffraction Data (<http://www.icdd.com/>).
13. G.de With, S. Harkema, D. Feil, *Acta Cryst.*, **1976**, B32, 3178.
14. P. J. Wheatley *Acta Cryst.* **1957**, 10, 182.
15. (a) K. Yvon, A. Bezinge, P. Tissot, P. Fischer, *J. Solid State Chem.* **1986**, 65, 225; (b) A. J. Salkind, W. C. Zeek, *J. Electrochem. Soc.* **1959**, 106, 366; (c) M. Jansen, P. Fischer, *J. Less Common Met.* **1988**, 137, 123.
16. W. P. Davey, *Phys. Rev.* **1925**, 25, 753.
17. I.-K. Suh, H. Ohta, Y. Waseda, *J. Mater. Sci.*, **1988**, 23, 757.
18. V. Petriček, M. Dušek, L. Palatinus **2006**. Jana2006. The crystallographic computing system. Institute of Physics, Praha, Czech Rep.
19. R. W. Cheary, A. A. Coelho, *J. Appl. Cryst.*, **1992**, 25, 109.
20. R.W. Cheary, A. A. Coelho, J. P. Cline, *J. Res. Natl. Inst. Stand. Technol.*, **2004**, 109, 1.
21. A. Kern, A. A. Coelho, R.W. Cheary, Chapter: "Convolution based profile fitting" in *Diffraction Analysis of the Microstructure of Materials*, edited by E. J. Mittemeijer & P. Scardi, Springer (**2004**), p. 17-49. ISBN 3-540-40510-4.
22. A. A. Coelho, *J. Appl. Cryst.*, **2000**, 33, 899.
23. P. E. Werner, L. Eriksson, M. Westdahl, *J. Appl. Cryst.*, **1985**, 18, 367.
24. A. Boultaf, D. Louër, *J. Appl. Cryst.*, **1991**, 24, 987.
25. J. W. Visser, *J. Appl. Cryst.*, **1969**, 2, 89.
26. M. Neumann, *J. Appl. Cryst.*, **2003**, 36, 356.
27. A. Le Bail, H. Duroy, J. L. Fourquet, *Mater. Res. Bull.* **1988**, 23, 447.
28. G. S. Pawley, *J. Appl. Cryst.* **1981**, 14, 357.
29. Materials Studio ver. 5.0, Accelrys Software Inc., USA **2009**.
30. Bruker AXS **2003**: TOPAS V2.1: General profile and structure analysis software for powder diffraction data. - User's Manual, Bruker AXS, Karlsruhe, Germany.
31. G. Kresse, *J. Furthmüller Phys. Rev. B* **1996**, 54, 11169.
32. P. E. Blöch *Phys. Rev. B* **1994**, 50, 17953.
33. D. Sun, C. -F. Yang, H. -R. Xu, H. -X. Zhao, Z. -H. Wei, N. Zhang, L. -J. Yu, R. Huang, L. Zheng, *Chem. Comm.* **2010**, 46, 8168.
34. P. C. Leung, *F. Aubke Inorg. Chem.*, **1978**, 17, 1765-1772.
35. Z. Mazej, E. Goresnik, Pacificchem; The International Chemical Congress of Pacific Basin Societies, Honolulu USA **2010**.
36. D. Sun, C. -F. Yang, H. -R. Xu, H. -X. Zhao, Z. -H. Wei, N. Zhang, L. -J. Yu, R. -B. Huang, L. -S. Zheng, *Chem. Commun.*, **2010**, 46, 8168.
37. D. Sun, N. Zhang, R. -B. Huang, L. -S. Zheng, *Crystal Growth & Design* **2010**, 10, 3699.
38. M. -H. Whangbo, H. -J. Koo, D. Dai, *J. Solid State Chem.* **2003**, 176, 417, and references therein.